Radioactivity and Gamma Spectroscopy

Duncan Beauch with Charlotte Hoelzl

April 19, 2022

Introduction

We are constantly bombarded with forms of radiation from space and materials all around us. Devices such as Geiger counters and scintillators can be used to measure this radiation from alpha, beta, and gamma decays.

Radioactive elements like the samples we will use in the following sets of experiments decay in well-defined processes, creating the same products each time. Using our Geiger counters and scintillators we can measure the energy of incoming radiation and determine its source.

In experiment 1 we will observe the full decay of an isotope and predict its half-life. In experiments 2 and 3 we will explore the attenuation of radiation through matter. In experiments 4 and 5 we will use a scintillator to view the full spectrum of radioactive samples and use statistical analysis to determine the types of decay products we detect.

Experiment 1: Half-Life of ^{137m}Ba

In this experiment we will measure the half-life of a sample of ^{137m}Ba, a relatively quickly decaying isotope produced from the decay of ^{137}Cs. Background data was recorded by the scintillation counter for several minutes while setting up the experiment to contextualize the barium readings. A diagram of the scintillation counter can be seen in Figure 1.

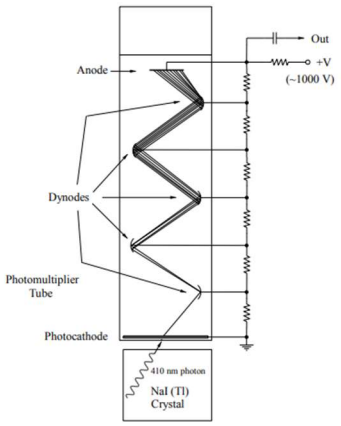

Figure 1: Scintillation Counter

A vial of 2ml of ^{137m}Ba from a ^{137}Cs generator was quickly placed in a tray just below the scintillation counter as close as possible. Counts immediately began to appear on the screen depicting a decay in the counting rate. Measurements were taken for approximately 20 minutes until the observed number of counts detected had decayed to roughly background levels. The data recorded can be seen in Figure 2.

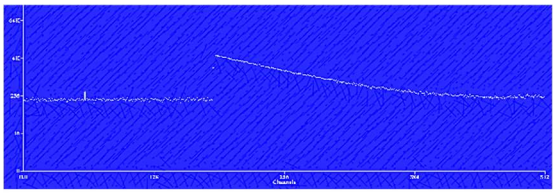

Figure 2: Decays detected by the decay of Ba137m

The average number of background counts was BG =195, which is within the expected range of about 150-200 counts in 4 seconds. Using this data, a plot of the natural log of the count C minus the average background BG was plotted as a function of time. The graph of $\ln(C - BG)$ vs. t which yields a straight line, whose slope is $-\lambda$, the decay rate constant for ^{137m}Ba. This plot

along with relevant statistics can be seen below in Figure 3.

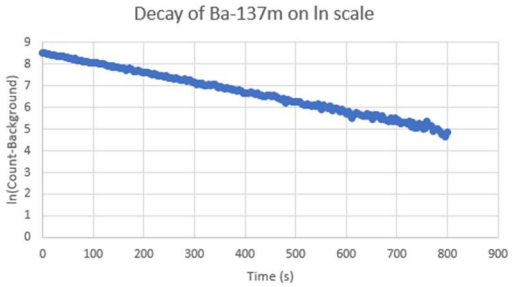

Figure 3: Linear regression for decay of Ba-137m. Slope = -0.004543 ± 0.000019

Using the calculated slope, we can calculate the half-life of ^{137m}Ba as

$$T_{1/2} = \ln\left(\frac{2}{\lambda}\right) = 152.57 \pm 0.92\ \text{s}$$

This is within a reasonable margin of the expected half-life of about 153 seconds.

Experiment 2: Absorption of Beta Particles

In this experiment we will use a sample of ^{137}Cs to measure the absorption of beta particles by varying thicknesses of copper. ^{137}Cs produces both gamma and beta radiation which are recorded by a Geiger counter. However, since gammas are attenuated exponentially through an absorber, the gamma counts received by the Geiger counter can be accounted for and ignored.

A stack of ten one-mil copper foils is placed in the largest slot in the plastic holder with three ten-mil foils on top. The cesium source is placed on a plastic tray just below the stack of foils with Geiger counter on top of the holder and lowered until just above the top foil. Data was recorded with 40 mils of absorbers between the source and the counter over a 30 second interval. After recording with 40 mils, the top foil was removed, so the thickness was 30 mils. This was repeated for absorber thicknesses of 40, 30, 20, 10, 9, 8, 7, 6, 5, 4, 3, 2, 1, 0. At a particular thickness, the foils stop all beta particles from reaching the counter, so the highest thicknesses are only allowing gamma particles as well as background radiation to reach the counter. However, there is a point where the highest energy beta particles are allowed through and each successive removed layer allows lower energy particles through, causing the number of counts to quickly increase with each reduction of thickness. The data and statistics recorded from this process can be seen in Figure 4.

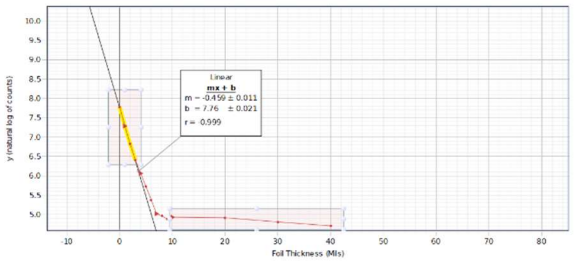

Figure 4: Absorption of beta emission from Cs-137 by varying thickness of copper

An estimate for the maximum range of the emitted beta particles can be obtained by fitting a line to the first four data points recorded and then fitting a second line to the last few data points. The thickness corresponding to the intersection point between these two lines is the maximum range which beta particles can penetrate. This intersection point yields a thickness of 6.03 ± 0.14 mils necessary to stop all beta particles from reaching the detector. This is slightly lower than the calculated value of 7 mils. However, errors can be attributed to limitations in the precision of the measurements, such as the thicknesses of the foils and accuracy of the counter.

Experiment 3: Attenuation of Gammas

In the previous experiment we claimed that gamma radiation attenuates exponentially with absorber thickness. In this experiment we will demonstrate that fact using known gamma radiation of 662 keV produced by a ^{137}Cs source through brass. Using the same scintillation counter from experiment 1, we will record gamma counts and model the attenuation of gamma radiation for varying thicknesses.

The cesium source is placed on the lowest tray of the holder, as far away from the counter as possible. The net count of 662 keV gammas that reach the detectors are recorded and not any lower energy rays over a 20-second period. This process is repeated thicknesses of 125-mil thick brass plate, incremented by 125-mil brass plates up to 1,125 net mils.

Plotting ln(net counts) vs. absorber thickness yields a slope corresponding to the linear absorption coefficient which can be used to find the half-thickness of brass. The graph and relevant calculations are shown below in Figure 5.

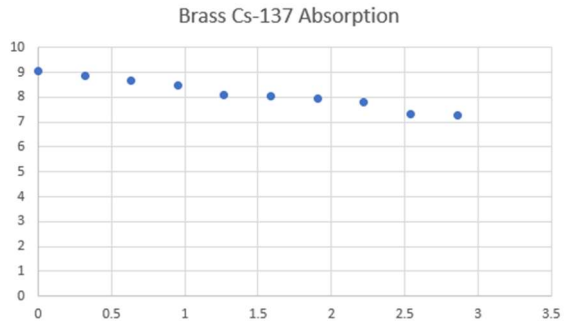

Figure 5: Plot of ln(net counts vs. absorber thickness (inch) for Cs-137 through brass absorber plates. Slope μ = 0.627 ± 0.034

The slope represents the linear absorption coefficient $-\mu = 0.627 \pm 0.034$ cm^{-1} and the half-thickness of brass can be calculated:

$$x_{1/2} = \ln\left(\frac{2}{\mu}\right) = 1.105 \pm 0.086\ cm.$$

This value is close to the theoretical value of $x_{1/2} = 1.21$ cm.

Experiment 4: High Energy Decay

In the following procedures we will be exploring the gamma spectrum of various radioactive samples in the ranges above 300 keV. We calibrate the scintillation counter for this higher energy range using a ^{22}Na source, where the two known energies of its gamma emission are 511 keV and 1,274 keV. The sample is placed directly in contact with the scintillator crystal and data is collected for 120 seconds. The statistics and notable portions of the plot such as the centroid, full-width at half maximum Γ (FWHM), and standard deviation σ (SD) of the full-energy peak as well as the Compton edge and backscatter peak. These statistics are reported for each sample in their relevant table below.

Table 1: Na-22 Spectrum for 511 keV

Characteristic	*Energy (keV)*
Centroid	511.053
FWHM	46.074
Compton Edge	337.144
Backscatter Peak	170.406
Full-Energy SD	19.566

Table 2: Na-22 Spectrum for 1274 keV

Characteristic	*Energy (keV)*
Centroid	1274.532
FWHM	54.061
Compton Edge	1049.154
Backscatter Peak	207.768
Full-Energy SD	22.958

Table 3: Cs-137 Spectrum	
Characteristic	*Energy (keV)*
Centroid	668.816
FWHM	50.989
Compton Edge	491.955
Backscatter Peak	203.263
Full-Energy SD	21.653

Table 4: Co-60 Spectrum for 1173 keV	
Characteristic	*Energy (keV)*
Centroid	1178.859
FWHM	58.975
Compton Edge	973.591
Backscatter Peak	220.978
Full-Energy SD	25.044

Table 5: Co-60 Spectrum for 1333 keV	
Characteristic	*Energy (keV)*
Centroid	1341.069
FWHM	59.59
Compton Edge	973.591
Backscatter Peak	220.978
Full-Energy SD	25.31

Table 6: Mn-54 Spectrum	
Characteristic	*Energy (keV)*
Centroid	841.749
FWHM	59.59
Compton Edge	648.61
Backscatter Peak	199.690
Full-Energy SD	25.31

Table 7: Zn-65 Spectrum	
Characteristic	*Energy (keV)*
Centroid	1118.583
FWHM	63.89
Compton Edge	923.83
Backscatter Peak	209.913
Full-Energy SD	27.13

The full-energy standard deviation is calculated as:

$$\sigma = \frac{\Gamma}{2\sqrt{2\ln(2)}}$$

We can use σ for the Na-22, Cs-137, and Mn-54 spectra to find the mean number of photoelectrons per unit energy deposited in the detector crystal dn_{pe}/dE_{dep} by plotting σ^2 vs. full-energy centroid. The plot for which is shown in Figure 6.

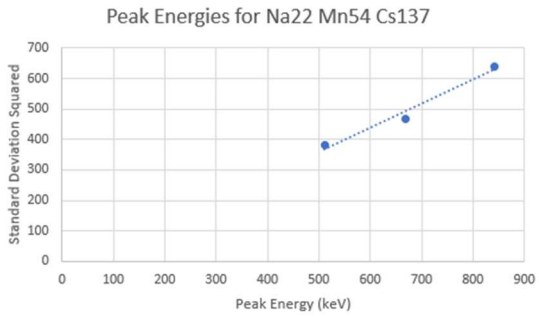

Figure 6: Plot of SD squared vs. peak for full energy spectrums

This gives a slope of dn_{pe}/dE_{dep} = 1.28 ± 0.21, which is within two standard deviations of the expected value.

Experiment 5: Low Energy Decay

Exactly the same as the previous experiment we will produce isotope spectra for various samples using a scintillation counter. However, this time we use a ^{109}Cd source to calibrate the energy scale which emits an 88 keV gamma and a 22 keV x-ray. We must also remove the detector from the lead shield in order to eliminate lead x-rays in the spectra calibrate the detector for lower energies.

With the detector calibrated, a ^{133}Ba sample is placed directly on the detector. Three peaks in addition to the expected peaks at 31 keV and 81 keV x-rays from the

decay of ^{133}Ba to ^{133}Cs. These peaks can be attributed to the sum peaks of these two x-rays as they come into the detector. Specifically, the combinations of two 31 keV, two 81 keV, and a 31 and 81 keV x-rays.

Now positioning a sample of ^{137}Cs directly on the detector, we can observe the low-energy spectrum of cesium. There are two peaks in this range whose statistics can be seen in Tables 8 and 9.

Table 8: Cs-137 Spectrum for 32 keV

Characteristic	*Energy (keV)*
Centroid	32.643
FWHM	7.704
Full-Energy SD	3.272

Table 9: Cs-137 Spectrum for 184 keV

Characteristic	*Energy (keV)*
Centroid	195.217
FWHM	1.744
Full-Energy SD	0.7406

In the previous experiments we have been using a lead shield around the detector to reduce unnecessary background noise. However, as our samples decay their products interact with the lead which produces x-rays. To measure this difference, we will compare the plots of low energy ^{137}Cs with and without the lead shield. These plots can be seen in Figures 7 and 8.

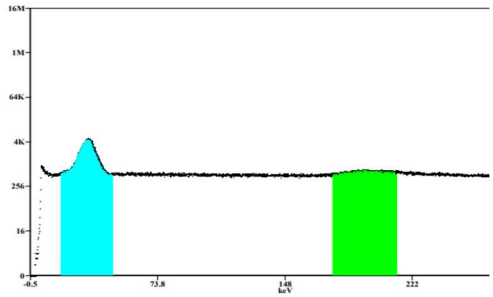

Figure 7: Cs-137 low energy spectrum without lead shielding

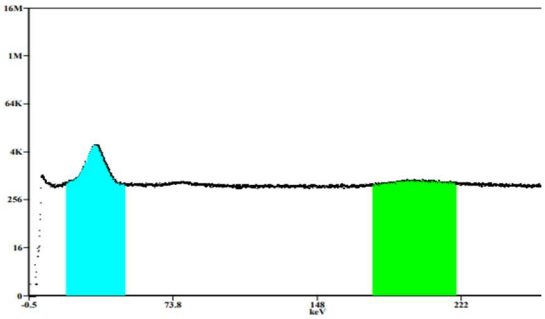

Figure 8: Cs-137 low energy spectrum with lead shielding

As expected, there is one additional peak in this spectrum, located at 78.5 keV. This spike is the x-ray emitted by lead exposure.

Conclusion

In these experiments we have explored the decay processes of various radioactive elements. We have shown that over long periods of time with respect to their half-lives we can predict their half-lives and observe the different decays occurring in the element. Although our graphs appear as peaks theoretically centered on the exact energy of the emitted product, these products do have well-defined energies. The variation in the measurements come from the measurement techniques used to probe the processes and using statistical analysis can confirm theoretical values as done in this report.

In experiment 1 we proved that the decay of ^{137}Ba can be modeled as an exponential function and its half-life extracted recording the counts received from a scintillator.

In experiments 2 and 3 we found how beta and gamma radiation interact with matter. For beta particles we found that the thickness it can penetrate is a linear function of the particle's energy. For gamma however, the thickness it can penetrate is an

exponential function of its energy, thus showing gamma radiation is much more difficult to interrupt.

In experiment 4, we used gamma spectroscopy to find the amount of energy deposited by gamma radiation into our detector crystal. In experiment 5, we used the low-energy spectrum of ^{137}Cs to probe the effect of lead shielding on our measurement devices. In both of these experiments we proved that statistical analysis of radioactive decay effectively produces the theoretical results we sought to confirm.